

---

# TREELEARN: A COMPREHENSIVE DEEP LEARNING METHOD FOR SEGMENTING INDIVIDUAL TREES FROM GROUND-BASED LIDAR FOREST POINT CLOUDS

---

Jonathan Henrich<sup>1,\*</sup>, Jan van Delden<sup>2,\*</sup>, Dominik Seidel<sup>3</sup>, Thomas Kneib<sup>1</sup>, and Alexander Ecker<sup>2,4</sup>

<sup>1</sup>Chairs of Statistics and Econometrics, Faculty of Economics, University of Göttingen

<sup>2</sup>Institute of Computer Science, University of Göttingen

<sup>3</sup>Department Spatial Structures and Digitization of Forests, Faculty of Forest Science, University of Göttingen

<sup>4</sup>Campus Institute Data Science, University of Göttingen and Max Planck Institute for Dynamics and Self-Organization, Göttingen

## ABSTRACT

Laser-scanned point clouds of forests make it possible to extract valuable information for forest management. To consider single trees, a forest point cloud needs to be segmented into individual tree point clouds. Existing segmentation methods are usually based on hand-crafted algorithms, such as identifying trunks and growing trees from them, and face difficulties in dense forests with overlapping tree crowns. In this study, we propose TreeLearn, a deep learning-based approach for tree instance segmentation of forest point clouds. Unlike previous methods, TreeLearn is trained on already segmented point clouds in a data-driven manner, making it less reliant on predefined features and algorithms. Furthermore, TreeLearn is implemented as a fully automatic pipeline and does not rely on extensive hyperparameter tuning, which makes it easy to use. Additionally, we introduce a new manually segmented benchmark forest dataset containing 156 full trees, and 79 partial trees, that have been cleanly segmented by hand. The data is generated by mobile laser scanning and contributes to create a larger and more diverse data basis for model development and fine-grained instance segmentation evaluation. We trained TreeLearn on forest point clouds of 6665 trees, labeled using the Lidar360 software. An evaluation on the benchmark dataset shows that TreeLearn performs equally well or better than the algorithm used to generate its training data. Furthermore, the method's performance can be vastly improved by fine-tuning on the cleanly labeled benchmark dataset. The TreeLearn code is available from <https://github.com/ecker-lab/TreeLearn>. The data as well as trained models can be found at <https://doi.org/10.25625/VPMPID>.

**Keywords** Tree Segmentation · Tree Extraction · Tree Isolation · LiDAR · MLS · TLS

## 1 Introduction

Today, forests are not only exposed to an ever-growing pressure from human use but also to a rapidly changing environment due to climate change. To understand changes in forest composition and structure as a response to these stressors, as well as for successful forest management, scientists and forest managers require precise and detailed information on the current status of our forests. To assess the structural characteristics of forests or individual trees, laser scanning techniques are a powerful tool [1]–[3]. They allow to create high-resolution 3D point clouds of the surfaces in a forest. To analyze such data, it is useful to separate the point cloud into the individual trees (Figure 1a), e.g. to classify them by their species [4]–[6] or to estimate the above-ground biomass [7], [8]. Separating a point cloud into individual trees is an instance segmentation problem: tree points must first be identified in the point cloud

---

\*The first two authors contributed equally to this work.



Figure 1: (a): predictions generated by TreeLearn on the benchmark forest dataset. (b): a top-view of the manually segmented benchmark forest dataset. For the green area at the edge there are no segmentation labels. It is still included in the dataset since it provides relevant context information for the labeled segment.

and then each point must be assigned to an individual tree instance. Since manually segmenting forest point clouds is highly time-consuming and subjective, there is a need for methods that automate this process. The method proposed in this work tackles this task for point clouds acquired using laser scanners located below the forest canopy. Primary sources of such point clouds are terrestrial and mobile laser scanning (TLS and MLS). Point clouds obtained by solely scanning from above the forest canopy usually do not capture the lower parts of the forest in high detail and therefore require a different set of methods, e.g. [9], [10].

The automatic segmentation of MLS and TLS point clouds into individual tree instances is a relatively young research field that has so far been mostly tackled by algorithms based on hand-crafted features. These algorithms usually first identify tree trunks and then assign the remaining points to these trunks based on a fixed set of rules. In early works, these rules were relatively simple. For example, some authors divided the point cloud into clusters and merged them based on distance and relative orientation [11], [12]. Follow-up work building upon these methods included more elaborate local geometry and shape features [13]. More recently, Fu *et al.* [14] avoided complicated feature computations and proposed to cluster trees from bottom to top in a layer-by-layer manner. Another strand of literature conceptualized the forest as a graph and segmented trees via graph cut [15]–[17] or graph pathing methods [18]. Furthermore, some works aimed to incorporate biological theories. For example, Liu *et al.* [19] constructed features based on plant morphology theory which were then used in a region-growing approach. Similarly, Tao *et al.* [20] developed a shortest-path algorithm based on metabolic theory, which states that plants tend to minimize the transferring distance to the root. Wang [21] also employed metabolic theory by constructing a superpoint graph where the node features depend on shortest path analysis. Recently, Xu *et al.* [22] proposed a segmentation method that identifies distinctive features in the forest and extracts individual trees based on topological structure. Compared to previous approaches, the method is more convenient for practitioners as it reduces the need for intensive hyperparameter tuning.

Although modern frameworks achieved significant improvements in performance, automated tree instance segmentation remains prone to errors and usually requires manual postprocessing [23], especially in dense forests with heavily intersecting tree crowns. In such scenarios, hand-crafted features and pre-defined heuristics appear to be too inflexible to account for the plethora of possible interactions between trees. Machine learning approaches could overcome these limitations, since features and association rules are derived directly from the data through gradient-based learning. In fact, recent advances in point cloud processing have been dominated by machine learning methods, as indicated by their performance on various point cloud processing benchmarks, e.g. [24]–[26].

Although machine learning methods have been applied to the segmentation of trees from forest point clouds [27]–[30], they mostly rely on projections into 2D. As a result, they lose information, because the network does not operate on the original point cloud. Other works do employ 3D deep learning for semantic segmentation, but resort to classical algorithms for tree instance segmentation [31]–[34]. To our knowledge, there are only a few studies in the related field of urban tree segmentation that actually employ 3D deep learning methods for tree instance segmentation [35], [36]. Furthermore, one concurrent work [37] recently showed the potential of directly performing deep-learning-based instance segmentation on forest point clouds. It is surprising that this research direction has not been explored more thoroughly since state-of-the-art instance segmentation methods for 3D point clouds exclusively operate on 3D input data [38]–[43], making them promising candidates for improving existing tree segmentation methods. In this paper, we adapt one of these methods [39] and propose TreeLearn, a comprehensive deep learning method to segment trees from forest point clouds. Our method first identifies tree points in the point cloud, then projects them towards the

respective tree base, and groups them via density-based clustering. The whole process is realized in an automatic pipeline which can be used out-of-the-box without extensive hyperparameter tuning. This reduces the number of work steps required to be performed by the user to a minimum, which makes our method easy to apply.

Since data-driven deep learning methods require large amounts of data for parameter optimization, high-quality labeled forest point clouds are urgently needed. Although there are some studies that use forest point clouds with manually corrected segmentation labels, some of them do not make their datasets public [16], [17]. Furthermore, those studies that provide publicly available datasets [10], [44]–[47] often have properties which limit their use for training machine learning methods. For example, Calders [44] only provides segmentation labels for a small number of trees located within a larger forest plot without segmentation labels. Weiser *et al.* [45] acknowledge quality limitations of their tree segmentations as well as low laser scanning coverage. Other studies only provide labeled trees instead of the complete point clouds [10], [46]. We argue that machine learning methods should be able to handle the complete registered point clouds to make its usage as easy as possible for practitioners. Furthermore, the separation of tree points from understory and ground points is often non-trivial and therefore itself an interesting training objective. A concurrent work [47] acknowledges the need for complete labeled forest point clouds by providing a large-scale dataset with high-quality semantic and instance segmentations of 1130 trees. In our work, we also provide a benchmark dataset of a continuous forest with high-quality crown segmentations and classification of points into non-tree and tree. It contains 156 trees that are completely and 79 trees that are partly within the labeled forest area (Figure 1b). Since forest types as well as laser scanning characteristics are diverse, we argue that every labeled forest point cloud is an important step to create a rich data basis for the development of powerful and general machine-learning-based tree segmentation algorithms. Additionally, the dataset can be used to systematically evaluate and compare existing methods. In summary, our study has two main contributions:

- TreeLearn, a fully automatic deep-learning-based pipeline that takes forest point clouds as input, identifies tree points, and groups them into individual trees.
- A high-quality hand-segmented forest dataset that can be used to train and systematically evaluate machine learning methods for tree segmentation.

## 2 Dataset

In Section 2 and Section 3, we describe the dataset and our TreeLearn pipeline in detail. Readers unfamiliar with the technical background can skip directly to the results section.

### 2.1 Scanning Areas

The data basis for model training and validation consists of MLS point clouds from 19 forest plots located in Germany. Eight plots are located near the city of Göttingen, in Lower Saxony, two near Allstedt in Saxony-Anhalt, two near Oppershofen in Hesse, and seven near Lübeck in Schleswig-Holstein. The stands are all dominated by European beech (*Fagus sylvatica* L.) and between 92 and 162 years of age. A detailed description can be found in [48]. The size of the study plots ranged from 0.9 to 2.2 ha.

### 2.2 Data Acquisition

The plots were recorded in February 2021, in leaf-less condition, using a ZEB Horizon mobile laser scanner (Geoslam Ltd., Nottingham, UK). The device uses a laser to measure the distance and direction to surrounding objects while being carried through a scene. Based on the principle of simultaneous localization and mapping (SLAM) the ZEB Horizon creates a 3D point cloud of the scenery up to a distance of 100 m from the walking trajectory of the operator. Each hand-held walkthrough with the scanner resulted in a file that was used to create a point cloud by conducting the spatial coregistration (actual SLAM) in GeoSlam HUB Version 6 [49]. The resulting point clouds were subsampled to 1 cm resolution to reduce scan artifacts. Additionally, noise filtering was conducted to remove points that are not of interest, such as scanned particles in the air.

### 2.3 Segmentation Labels

To train the neural network in a data-driven manner, already segmented forest point clouds are required. We obtained our segmentation labels for the forest point clouds in two ways: (1) by using the automatic segmentation functionality provided by the Lidar360 software [50] and (2) by manually correcting the segmentation labels of a single forest plot. The automatic segmentation labels were used for training, while the manually corrected labels were used for fine-tuning and evaluation.

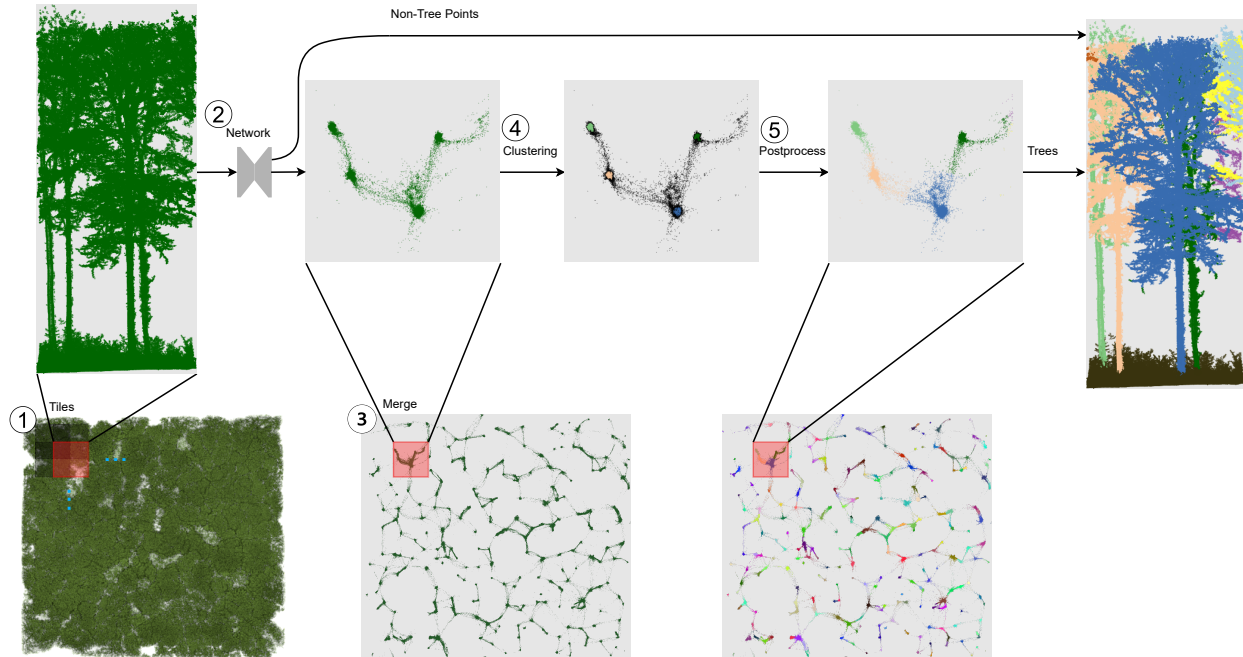


Figure 2: The pipeline for segmenting a forest point cloud. The circled numbers correspond to the five steps of the pipeline described in Section 3.

**Automatic segmentation** To automatically segment the 19 forest point clouds into individual trees, we used the TLS-package from Lidar360 as described by Neudam *et al.* [48]. The hyperparameters of the Lidar360 software were optimized to produce visually appealing tree segmentations. A minimum size of 10 m was chosen as a requirement for tree classification. Consequently, vegetation that is smaller than 10 m or points belonging to the forest ground were classified as non-tree points. Lidar360’s segmentation algorithm operates on a point cloud that is terrain-normalized, i. e. has a flat ground surface. This was achieved in a separate preprocessing step. To bypass the need for terrain normalization for our method, labels from the terrain-normalized data were transferred to the original data. The automatic segmentation contains numerous errors, including multiple trees detected as a single tree, non-tree points identified as part of trees, and inaccuracies in discerning tree boundaries in crowns and branches that are close to each other. Since these labels contain numerous mistakes, we refer to them as noisy labels. The noisy labels were used for training since individual trees are roughly captured correctly. The model obtained from training on these noisy labels serves as a starting point for fine-tuning.

**Manually corrected segmentation** For one forest plot, we manually corrected the segmentation labels generated by Lidar360 with the help of CloudCompare [51] by comparing each tree to all surrounding trees. In a first step, all trees were assessed and corrected if necessary. In a second step, these segmentations were verified and potentially refined. This was done by two authors (J. H. and J. v. D.). The corrected segmentation covers an area of 112 m by 103 m. It includes 235 trees, 156 of which are located entirely within the segment and 79 of which are partly within the segment (Figure 1b). We appended 11 m of the unlabeled forest point cloud to the labeled segment (Figure 1b, green area at the edge). This area is included in the dataset since it provides relevant context information for the manually segmented parts. The ratio of non-tree to tree points in the dataset is approximately 2:3. We make the forest plots employed in this work along with the generated segmentation labels available from <https://doi.org/10.25625/VPMPID>.

### 3 TreeLearn Pipeline

The goal of our TreeLearn pipeline is to identify the points belonging to trees in a 3D forest point cloud and then group these points into individual trees (Figure 2). More precisely, given a set of 3D points  $P = \{p_i = (x_i, y_i, z_i)\}_{i=1}^N$ , our pipeline tackles the tasks of semantic and instance segmentation. The goal of semantic segmentation is to achieve a partition of all points into tree and non-tree points by assigning each point  $p_i$  to one of the two classes. The non-tree class includes all points belonging to the forest ground and smaller vegetation such as bushes or trees smaller than



10 m. The tree class includes all points belonging to trees larger than 10 m. The goal of the instance segmentation step is to partition the tree points into  $K$  (mutually exclusive) individual tree instances. The number of instances  $K$  is not known a-priori and must be determined dynamically depending on the input data. The pipeline consists of the following five steps (Figure 2):

1. Divide the forest point cloud into smaller overlapping rectangular tiles based on the x- and y-coordinates to handle memory restrictions.
2. Use a neural network to predict two quantities for each point in a tile: (1) an offset vector pointing towards the x- and y-coordinates of the tree base (Figure 3a), and (2) a semantic score indicating the probability that a point belongs to a tree or not. This step is carried out separately for each tile generated in step 1.
3. Merge the predictions for the individual tiles to obtain semantic and offset predictions for the whole input point cloud. Project the point coordinates by adding the offset.
4. Apply a clustering algorithm on these projected coordinates to partition the points into individual trees. Disregard points that are not predicted to be tree points.
5. Postprocessing: assign the remaining tree points that have not yet been assigned to a tree in step 4 by using a nearest-neighbor criterion.

Running the complete TreeLearn pipeline on our 112 m by 103 m benchmark dataset takes about 180 minutes (3 GHz CPU; 16 physical cores of which one to two are used). The runtime is primarily determined by the CPU, since most time is spent in step one of the pipeline which includes feature calculation (30 minutes) and generating tiles and filtering them (100 minutes). GPU calculations require roughly 9 GB of memory and runtime is negligible. The runtime scales roughly linearly with the area of the plot.

### 3.1 Step 1: Generate Overlapping Forest Tiles

The point clouds of an entire forest plot in our datasets contain around 20 000 000 points. Processing a point cloud of this size at once using a neural network is infeasible due to memory restrictions. To address this issue, we employ a sliding window approach to process the forest. Predictions are generated for smaller, overlapping tiles that can be processed by the neural network. This approach is inspired by Ronneberger *et al.* [52] who proposed tiling to process large input images. To create the tiles, we cut out rectangular sections with a fixed edge length of 30 m along the x- and y-axis from the original forest point cloud. The edge length along the z-axis is determined by the highest point. The tiles are generated in an overlapping way with a stride of 4 m. For each point within a tile, we calculate a feature that describes the local verticality of the point cloud [53], which is later used for clustering purposes (see Section 3.4).

Prior to generating the tiles, the lidar scans are subsampled with a voxel size of  $10\text{cm}^3$ , leaving only one point within a voxel. We argue that resolutions above 10 cm are not necessary for a large-scale task like tree segmentation. The tiles are further filtered using statistical and radius outlier removal [54]. The subsampling and filtering is designed to yield tiles with a reduced number of points to lower the computational demand, while at the same time preserving the complex structure of trees. Furthermore, the procedure is likely to produce similar results for data obtained by different laser scanners. For example, different laser scanner resolutions above 10 cm do not have an influence on the input data due to the subsampling procedure. This makes our method robust against changes in the input point cloud.

Two things should be noted: first, due to the subsampling and filtering, our algorithm does not operate on the original point cloud. However, results on the original point cloud can be easily obtained by propagating the predictions from the filtered and subsampled point cloud to the original one, e.g. using k-nearest neighbors. Second, the tiling procedure can also be employed if the input point cloud is not rectangular. In fact, our method can be employed on arbitrarily shaped input point clouds.

### 3.2 Step 2: Predict Semantic Scores and Offsets

After having generated smaller processable point clouds, we use a neural network to predict two quantities for every point: first, we predict the probability that a point belongs to the semantic classes tree or non-tree. As these classes are mutually exclusive, this is a binary classification problem. Second, for every point we predict an offset vector [55] that points towards the x- and y-coordinates of the tree base. Specifically, the tree base is defined as the location of the trunk at a height of three meters. At this height, tree trunks are often further apart from neighboring close trunks than at the bottom. Figure 3a visualizes the offset vectors for a few example points.

Without any modifications, we use a well established neural network architecture that has been proven to be a powerful backbone for 3D scene understanding tasks [38], [39], [41]. The focus in this work is not on the network itself, but rather on its integration in a comprehensive segmentation pipeline. The network that we use for semantic and offset

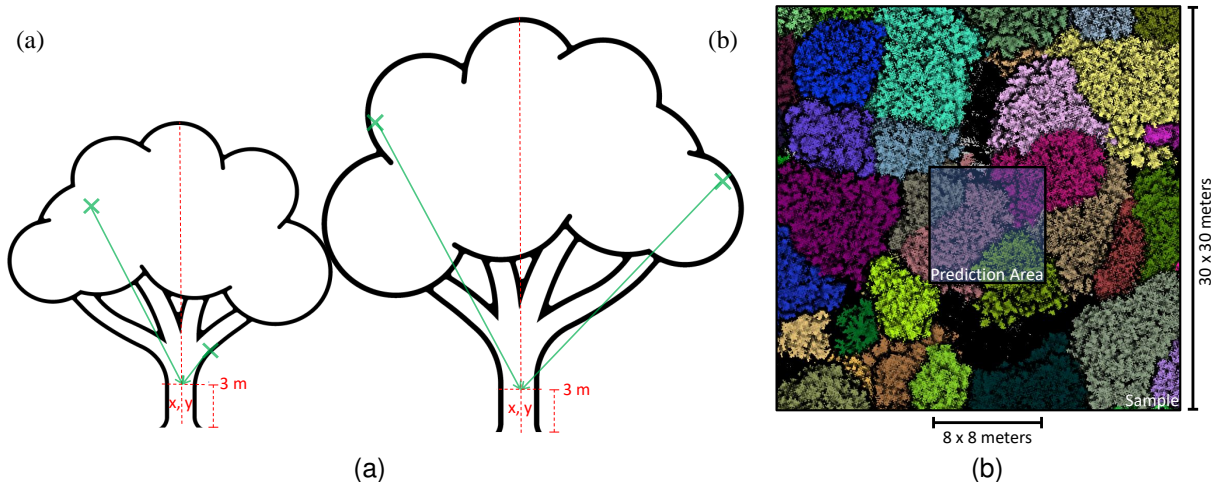


Figure 3: Visualizations regarding offset prediction. (a) depicts offsets for two example trees. The offset is the vector from a point towards the  $x$ - and  $y$ -coordinates of the tree base. The tree base is defined as the location of the trunk at a height of three meters. (b) visualizes the prediction area in relation to the whole tile. To make sure that the network has the necessary context information, predictions are only produced for the inner blue area of the tile.

prediction takes as input a sparse voxel grid. First, the input space is partitioned into a 3D voxel grid where each voxel is  $10\text{ m}^3$  in size. Then, for each voxel it is checked whether it contains at least one point. If it does, the voxel is active and will be considered as part of the input to the network. Only active voxels are stored. All other voxels are ignored, hence the name 'sparse voxel grid'.

The network is a variant of the original U-Net introduced by Ronneberger *et al.* [52]. The structure of a U-Net can be divided into two main steps. In the contraction step, features are computed in a hierarchical manner by gradually taking into account an increasingly larger context. In the expansion step, these features are propagated to the original points to arrive at rich voxel features that are used for semantic and offset prediction. For a more detailed explanation of the principles, we refer to the original paper [52]. Compared to the original U-Net, the network employed in this work follows the sparse convolution design proposed by Graham *et al.* [56]. Sparse convolutions differ from regular convolutions in that an activation in the output feature channel occurs only if the voxel at the center of the convolution kernel contains a point. This keeps the number of activations constant, which avoids excessive memory consumption. Furthermore, instead of just stacking convolutions, residual blocks are used to facilitate gradient flow [57]. The residual blocks consist of two  $3 \times 3$  convolutions and a residual connection. Each contraction step of the U-Net consists of two residual blocks and a  $2 \times 2$  learned pooling layer implemented by a convolution with stride two. In this work, we employ seven contraction steps. During expansion, it is ensured that the sparse structure is preserved by only propagating activations to voxels that were active during the corresponding contraction step [58].

To predict the offset and semantic class, two separate heads are used, each of which take as input point features  $F$ . These point features  $F = \{f_1, \dots, f_N\} \in \mathbb{R}^{N \times D}$  are obtained from the U-Net output by extracting for each of the  $N$  original points the corresponding  $D$ -dimensional voxel feature. The semantic head maps onto semantic scores and consists of a multilayer perceptron (MLP) with two layers whose parameters are shared between points. Similarly, the offset head uses a shared three-layer MLP and maps onto offset predictions.

Accurate offset prediction is possible only if the corresponding tree base is within the input tile, so the network can detect it. We therefore predict offsets only for the central  $8\text{ m} \times 8\text{ m}$  portion of each tile, while the network still receives the whole  $30\text{ m} \times 30\text{ m}$  tile as input (Figure 3b). This approach ensures that the network has sufficient context information around the points for which it makes predictions. Semantic predictions are also generated only for the inner square.

### 3.3 Step 3: Merge Tiles

After semantic scores and offset vectors have been predicted for all tiles, the points from the inner squares along with their predictions are concatenated to obtain predictions for the full forest point clouds. No predictions are made for points outside the inner square. As the inner squares of neighboring tiles have an overlap of 4 m, multiple predictions for each point are generated. These predictions are then averaged, which reduces artifacts introduced by tiling and

leads to smoother transitions between tiles. We calculate the projected coordinates  $c_i = p_i + o_i$  by adding the predicted offsets ( $o_i$ ) to the original points ( $p_i$ ).

### 3.4 Step 4: Identify Tree Instances

Since the goal is to arrive at tree instances, we only consider points with a higher probability to belong to the semantic class tree in this step. If the offset prediction for these points was perfect, the projected coordinates  $c_i$  would have exactly the x- and y-coordinate of the corresponding tree base. In practice, the projected points that belong to the same tree still group together, but predictions are far from perfect. Projected points are often positioned in between neighboring high density areas that represent individual trees. These points form strings connecting the high density regions (Figure 2, see image at step 3). This is the result of prediction errors for points that cannot be clearly assigned to a tree, for example if the branches of two trees are heavily intertwined. In contrast, points belonging to the tree trunk have a much lower prediction uncertainty. Therefore, to obtain clearly separated tree clusters, we perform clustering only on points that fulfil the following two conditions: (1) the verticality feature of the point (see Section 3.1) has a sufficiently high value of  $\tau_{\text{vert}}$ , and (2) the absolute value of the z-component of the offset prediction is at most  $\tau_{\text{off}}$ . Condition (1) already separates trunk points from other tree points to a large degree. However, some points in tree crowns also have high local verticality. Therefore, condition (2) only selects those points that are sufficiently close to the tree base, thus ensuring that crown points are excluded from clustering.

Individual tree clusters are identified by using the projected coordinates  $c_i$  of the full forest point cloud that fulfil the verticality and offset condition above. These coordinates are used as input to a density-based clustering algorithm [59] following previous works [38], [39]. Specifically, an undirected graph is constructed where an edge between two points exists if their Euclidean distance is smaller than a predefined grouping radius  $\tau_{\text{group}}$ . Clusters are then obtained by identifying all connected components of the graph that consist of at least  $\tau_{\text{min}}$  points (Figure 2, see image at step 4). The z-coordinate is ignored during clustering. The selection of the specific values for all hyperparameters  $\tau$  used for instance identification is described in Section 4.3.

### 3.5 Step 5: Assign Remaining Points

In the previous step, tree instances have been identified but a large proportion of points has not yet been assigned to individual tree instances (Figure 2, black points on image at step 4). To assign these points, we opt to use a simple strategy: the  $k$  nearest neighbors of these points are determined among points that have already been assigned to trees. These neighbors are calculated based on the projected coordinates  $c_i$ . Therefore, the assignment of points to individual trees is done entirely based on information provided by the neural network. We set  $k = 10$ . Different values of  $k$  lead to highly similar results.

## 4 Training

The U-Net described in Section 3.2 was first trained using the noisy labels automatically obtained from Lidar360. The model obtained by training on noisy labels was then fine-tuned using the manually corrected clean labels.

### 4.1 Noisy Labels

To generate the training data, we cropped out random areas of size  $30 \text{ m} \times 30 \text{ m}$  from the 18 forest plots that have only been automatically segmented. For these crops, subsampling and filtering was then performed according to the procedure described in Section 3.1. In total, 20 000 crops were generated.

To train the network, we calculate loss values on the predictions within the inner area of a crop, as displayed in Figure 3b. This way, the neural network almost always has enough context information. To supervise the offset prediction, we use the average L2-distance across tree points between the actual and predicted offset vector. For the semantic predictions, we use the binary cross entropy loss function and further scale it by a factor of 50 to obtain a similar magnitude to the offset loss. The offset and semantic loss are then summed to obtain the loss used for training. The U-Net was trained for 150 000 iterations using the AdamW optimizer [60] with a weight decay of  $10^{-3}$  and  $\beta = [0.9, 0.999]$ . The batch size was set to 4. We further chose a cosine learning rate schedule [61] with a warm up period of 6250 iterations and a maximum/minimum learning rate of  $3 \times 10^{-3}/5 \times 10^{-6}$ . Parameters pre-trained for 3D instance segmentation from [62] were used as initialization for the model. Network training was performed on a single Nvidia RTX A5000 and took roughly 40 hours.

## 4.2 Clean Labels

Following the same procedure as described in Section 4.1, 4500 training crops were generated for the cleanly labeled forest plot. For fine-tuning, the model was initialized with parameters obtained by training with noisy labels. From there, the network was trained for 3125 iterations without warm up and a maximum/minimum learning rate of  $4 \times 10^{-5}/5 \times 10^{-7}$ . Otherwise, the training specifications were the same as described in Section 4. Fine-tuning was performed on a single Nvidia RTX A5000 and took roughly 2 hours. Apart from fine-tuning, training the model from scratch with cleanly labeled data was also attempted, but was not successful due to overfitting.

## 4.3 Model Selection

We had one cleanly labeled forest plot. To report unbiased estimates of model performance, we split it into two parts: one used for model selection (validation set) and the other one for estimating model performance (test set). To make the best use of the available data, we used each part once as the validation set and evaluated the performance on the other, and vice versa. When training with the noisy labels, the parameters with the lowest offset loss on the validation set were selected. The validation set was then also used to fine-tune the selected parameters as described in Section 4.2. In this case, the parameters after the last training iteration were selected without any selection criterion. This way, test performance on the full cleanly labeled forest plot can be evaluated for both noisy and clean label training.

For the density based clustering step described in Section 3.4, there are four hyperparameters. Two hyperparameters decide which points are considered in the clustering algorithm: the maximum vertical distance to the tree base was set to  $\tau_{\text{off}} = 2$  m and the minimum required verticality feature value was set to  $\tau_{\text{vert}} = 0.6$ . The verticality feature of a point can reach a maximum value of one for a perfectly vertical straight line of points. A value of 0.6 allows for slightly slanted trunks. A value of 2 m for the maximum vertical distance from the tree base further ensures that only trunk points are considered. There are two additional hyperparameters that govern the behavior of the clustering algorithm: first, the minimum number of points for a valid cluster was set to  $\tau_{\text{min}} = 100$ . This number was chosen based on considerations how many points a valid tree cluster might contain in extreme cases, e.g. when the tree trunk is very thin. Second, the grouping radius for clustering was set to  $\tau_{\text{group}} = 0.15$  m. In Appendix A, we analyze how the number of false positive and false negative predictions is influenced by different grouping radii  $\tau_{\text{group}}$ . Together with qualitative results obtained on an out-of-domain test dataset (see Section 6.2), this analysis suggests that our method can be employed out-of-the-box without extensive hyperparameter tuning.

# 5 Evaluation Metrics

## 5.1 Semantic Segmentation Evaluation: Tree vs. Non-Tree

For semantic segmentation evaluation, we assess how well the method divides the points into the semantic classes tree and non-tree. As a metric, we choose the accuracy, which is the number of correctly predicted points divided by the total number of points. We report evaluation results on the point cloud subsampled with a voxel size of  $10\text{cm}^3$  (see Section 3.1). This avoids a disproportionate weighting of regions with higher point densities like the trunks.

## 5.2 Instance Detection Evaluation

For instance detection evaluation, we are interested in how well the predicted tree instances match the ground truth tree instances. Specifically, we consider true positive predictions ( $TP$ ), false negative predictions ( $FN$ ) and false positive predictions ( $FP$ ) as defined by Fu *et al.* [14]: a tree prediction is  $TP$  if, in principle, it has a clear match (defined below) to a ground truth tree. If a tree is predicted to belong to a larger nearby tree or is not detected at all, it is  $FN$ . Finally, if a prediction is no complete tree instance but only a fragment, it is  $FP$ . It should be noted that one prediction consisting of two merged trees only results in one  $FN$ . The larger tree of the two still counts as detected using the above definition.

To automatically identify  $TP$ ,  $FP$  and  $FN$  predictions, we first calculate the pointwise intersection over union (IoU) between all predictions and ground truths. Then, Hungarian matching [63] is performed to assign predictions to ground truths. To avoid the assignment of fragments to ground truth trees, we set a minimum IoU of 0.3 as a requirement for a match. Matched predictions, non-matched predictions and non-matched ground truths are considered  $TP$ ,  $FP$  and  $FN$  respectively. Trees at the edge of the segmented area are often only partially within the point cloud and might consist of only one branch within the segmented area. If this one branch is falsely assigned to another tree, this results in a  $FN$ . This is misleading since the actual tree, which is not within the evaluation area, might be correctly detected. Therefore, we consider only trees that are fully within the prediction area (156 trees) for this part of the evaluation. Likewise, only predictions whose maximum overlap is with one of these 156 trees, are taken into account.

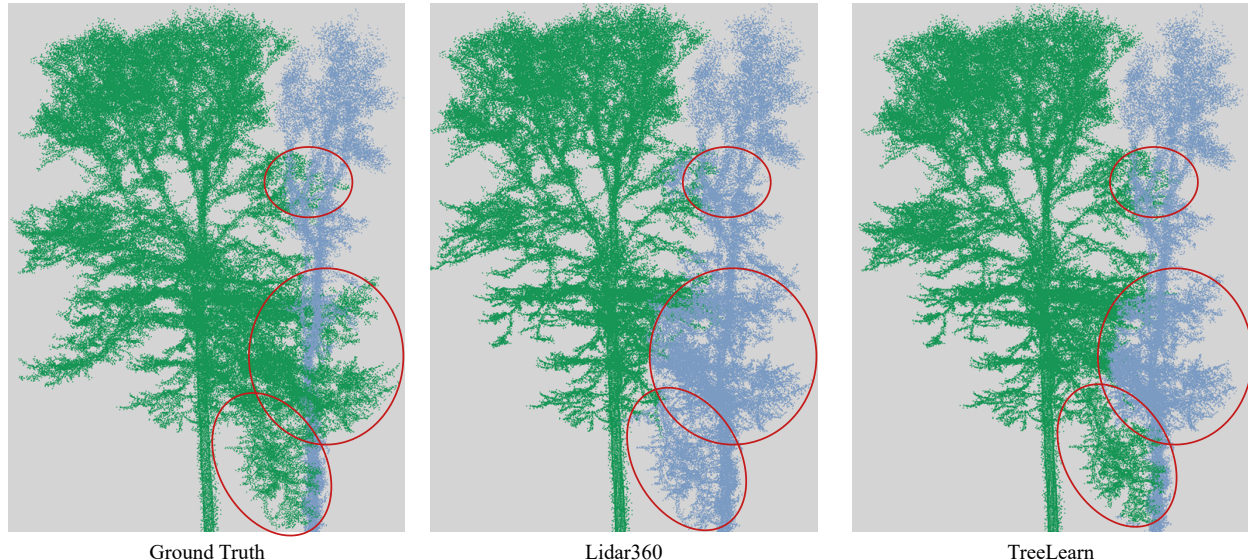


Figure 4: Comparison of instance segmentation results for two heavily intertwined trees. Areas of interest are marked with red circles. The result of TreeLearn has some errors, but is better than Lidar360.

### 5.3 Instance Segmentation Evaluation

For the evaluation of instance segmentation, we assess how well the points of the predicted tree instances match the points of the corresponding ground truth tree instances. This is different to instance detection (Section 5.2), in that we are not evaluating whether a specific tree is detected at all, but how well the individual points of a specific predicted tree match to the actual tree. Since detection errors represent a different quality of mistakes, we do not consider predicted tree instances that are associated with a detection error. This includes (1) *FP* predicted tree instances (fragments) and (2) predicted tree instances that consist of more than one ground truth tree (merged predictions). To evaluate the instance segmentation, we use precision, recall and the F1-score:

$$Prec = \frac{TP}{TP + FP} \quad Rec = \frac{TP}{TP + FN} \quad F1 = 2 * \frac{Prec * Rec}{Prec + Rec} \quad (1)$$

Note that *TP*, *FP* and *FN* are here defined at the point-level, not the instance-level. The metrics are calculated separately for every predicted tree instance with the corresponding ground truth tree points as positives and all other points as negatives. Then, they are averaged over all predictions that are taken into account.

Not all locations of a tree are equally difficult to segment correctly. For example, points near the trunk are usually easier to assign than points farther outside where there are many interactions with other trees. To quantify how well different parts of the trees are segmented, we partition the points of a prediction and the corresponding tree into 10 subsets and calculate the metric for each subset. For each subset, the metric is then averaged across predictions. We propose two axes for partitioning: (1) horizontal distance to the trunk, and (2) vertical distance to the forest ground. For the horizontal partition, the  $i$ -th subset contains all points with a horizontal distance to the trunk between  $\frac{i-1}{10}r$  and  $\frac{i}{10}r$  where  $r$  is the maximum distance. For the vertical partition, the  $i$ -th subset contains all points with a vertical distance to the ground between  $\frac{i-1}{10}h$  and  $\frac{i}{10}h$  where  $h$  is the height of the tree. We set  $i = 1, \dots, 10$ .

## 6 Results

TreeLearn performs three tasks: separating tree points from non-tree points, detecting individual trees and assigning points to their corresponding tree instance. In the following, we evaluate the system’s performance on each of these tasks using our manually labeled benchmark dataset and compare it with two existing methods: the commercial Lidar360 software [50] and TLS2trees [33], a recent open source graph-based instance segmentation method.

We trained TreeLearn supervised on labels generated automatically by Lidar360. The segmentation results of this software have mistakes, hence the need to improve. Our first, perhaps surprising, finding is that the segmentation



Table 1: Overall results. Instance segmentation results averaged across predictions. Semantic and instance segmentation results in %.

	Semantic Segmentation	Detection		Instance Segmentation
	Accuracy	<i>FP</i> Predictions	<i>FN</i> Trees	<i>F1</i>
TLS2trees <sup>a</sup>	98.9	0	0	88.39
Lidar360	99.6	1	1	93.23
Noisy Labels Training	99.69	0	0	93.98
Clean Labels Fine-tuning	<b>99.88</b>	1	0	<b>97.84</b>

<sup>a</sup>TLS2trees detects very small tree-like formations. For a fair comparison, these detections were manually assigned to the non-tree class since we only consider trees of at least 10 m height.

Table 2: Instance segmentation results averaged across predictions. All values in %.

	Precision	Recall	<i>F1</i>
TLS2trees	88.2	90.52	88.39
Lidar360	92.56	94.82	93.23
Noisy Labels Training	93.45	95.34	93.98
Clean Labels Fine-tuning	<b>97.57</b>	<b>98.28</b>	<b>97.84</b>

algorithm learned from these ‘noisy’ labels performs slightly better than the algorithm that generated the training data, i. e. a machine learning approach can extract more consistent segmentation rules than its ‘teacher’. On average, TreeLearn improves instance segmentation performance measured by the *F1*-score from 93.23 % (Lidar360) to 93.98 % (Table 1). TLS2trees achieves an *F1*-score of 88.39 %. TLS2trees was applied using the standard hyperparameters from the paper [33] to give an example of the out-of-the-box performance of another method. It should be noted that TLS2trees, unlike our model, has not been developed using the specific forest type and laser scanner used in this study. We expect the reported performance gap between the two methods to decrease for other settings.

Fine-tuning TreeLearn on the clean manually labeled forest plot improves the result drastically to an instance segmentation performance of 97.84 % (for an example, see Figure 4). Both variations of TreeLearn also produce a better separation of trees and non-tree points than Lidar360 and TLS2trees. In particular, the semantic segmentation accuracy increases from 99.6 % (Lidar360) to 99.88 % for the fine-tuned TreeLearn. Detection performance on our benchmark dataset is without errors for both TLS2trees and TreeLearn trained with noisy labels. In contrast, the fine-tuned TreeLearn and Lidar360 produce one prediction that does not actually constitute a tree (*FP*) and Lidar360 additionally fails to detect one tree (*FN*). However, detection errors are too rare on our benchmark dataset, so there is no conclusive evidence that one method performs better than the others in this regard.

## 6.1 Instance Segmentation

In this section, we take a more detailed look at the instance segmentation results. In addition to an overall better *F1*-score, both TreeLearn settings achieve a better precision and recall value than Lidar360 and TLS2trees (Table 2). We also observe that, irrespective of the method, recall is higher than precision. We conjecture that this is the case because the branches of larger trees often protrude into smaller trees. If these branches are then incorrectly assigned to the smaller tree, the precision of the smaller tree is affected considerably. On the other hand, a falsely assigned branch does not affect the recall of the larger tree to the same degree.

A more fine-grained understanding can be achieved by evaluating the segmentation performance at different locations of a tree. For this, we partition the points of a prediction and the corresponding tree into subsets based on horizontal distance to the tree trunk and vertical distance to the forest ground as described in Section 5.3. Figure 5 shows precision, recall and *F1*-scores for the two partitions. For all methods, performance decreases for points farther away from the trunk due to increased interactions with other trees. However, this trend is less pronounced for TreeLearn, indicating a certain stability with respect to the distance to the trunk. This is especially true for the fine-tuned model.

For the vertical partition of the trees, both TreeLearn and Lidar360 have a visible performance low for intermediate heights, where trees tend to have their maximum width. For TLS2Trees, this tendency is not observed. Furthermore,

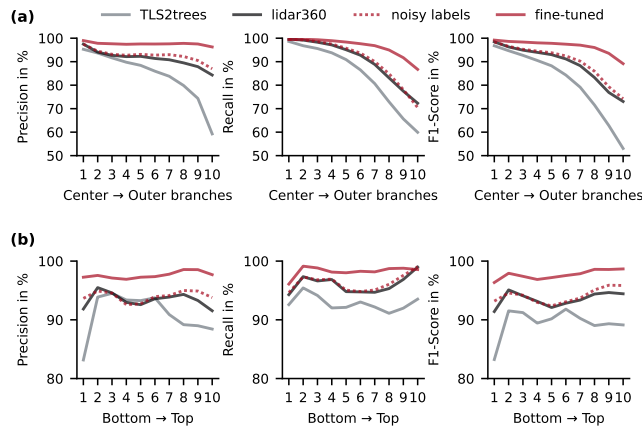


Figure 5: Instance segmentation performance. (a) shows metrics for segments along the x- and y- axis. (b) shows metrics for segments along the z-axis.

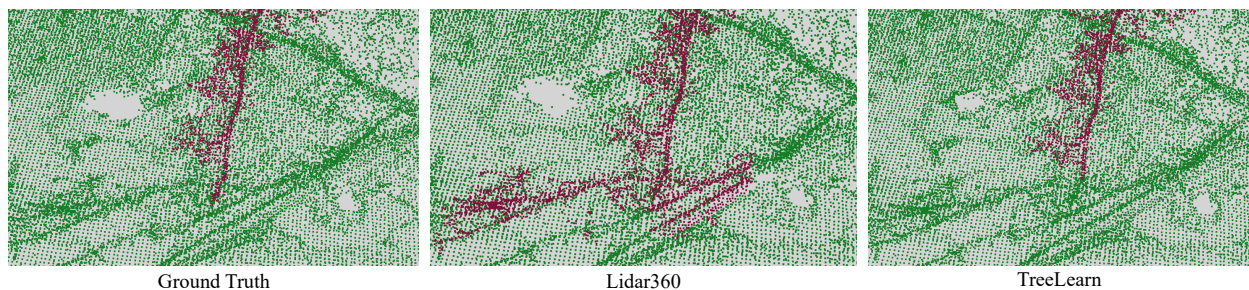


Figure 6: Comparison of semantic segmentation results. Green points are assigned to the non-tree class, red points to the tree class. Lidar360 assigns completely unrelated points to the tree class. TreeLearn is more accurate.

the area directly above the ground poses difficulties for all methods. This is most likely due to understory and tree points that are hard to distinguish from each other (see e.g. Figure 6).

## 6.2 Qualitative Test Results

In addition to the quantitative results on our benchmark dataset, we used our fine-tuned TreeLearn model to obtain qualitative results on a completely unrelated forest plot. Specifically, we used a forest point cloud from the Wytham Woods forest in Oxford, UK, that was kindly provided by the authors that introduced the dataset [10], [64]. This forest point cloud differs in the tree species composition and was scanned with a different laser scanner than our training data. Our method produces adequate segmentation results on this out-of-domain forest point cloud without any further hyperparameter tuning (Figure 7).

## 7 Conclusion

In this study, we introduced an automatic pipeline for segmenting individual trees from high-resolution forest point clouds, requiring no extensive hyperparameter tuning or data preprocessing in the form of ground and understory removal or terrain normalization. To the best of our knowledge, this work is, along with one concurrent work [37], the first to tackle this task with a deep learning method that operates directly on point cloud data. TreeLearn is based on a 3D U-Net for pointwise feature prediction, followed by clustering and postprocessing to derive instance predictions. As demonstrated in Section 6, our method performs equally well or better than Lidar360 in all aspects, despite being trained on data segmented by it. This highlights the potential of deep learning to replace more complex tree segmentation algorithms to reduce computational demands. Furthermore, our results indicate that major performance increases can be achieved by fine-tuning the network on small amounts of high-quality labeled data. In addition to the segmentation method, we introduced a new benchmark dataset that allows for model training and evaluation of



Figure 7: Segmentation result generated by TreeLearn on a point cloud from Wytham Woods forest.

instance segmentation results. This is an important step towards the creation and comparability of powerful deep-learning-based tree segmentation algorithms.

Future research should aim to incorporate TreeLearn in a more general forest inventory framework. Specifically, if adequate training data is available, our method offers the possibility to seamlessly integrate a more fine-grained semantic segmentation into ground, understory, woody parts and leaves, without any changes to the overall pipeline. Furthermore, limitations resulting from the training data used should be addressed. For example, our model was trained with crops with an edge buffer of 11 m where trees with a height of less than 10 m were labeled as non-trees. If trees that are wider than  $2 * 11 \text{ m} = 22 \text{ m}$  or smaller than 10 m should be correctly recognized, the training data must be adapted accordingly. Furthermore, only beech forests have been used during training. We expect a drop in performance when segmenting point clouds of forests with a highly different structure. Incorporating more diverse data during training or fine-tuning can alleviate this issue. On a positive note, this also means that the model can benefit from any tree segmentation dataset contribution made by the community. In future work, we plan to gather and train on forest data from previous works [10], [46], [47] in an effort to obtain more powerful and generalizable models independent of the characteristics of specific forests or laser scanners. The availability of such models is an important prerequisite for large-scale detailed forest inventory since forest scientists and managers crucially rely on single-tree point clouds for the extraction of single-tree parameters. Such data is urgently needed to plan silviculture activities, to estimate carbon stocks or harvest yields, and for many others tasks.

## References

- [1] X. Liang, J. Hyypä, A. Kukko, H. Kaartinen, A. Jaakkola, and X. Yu, “The use of a mobile laser scanning system for mapping large forest plots,” *IEEE Geosci. Remote Sens. Lett.*, vol. 11, no. 9, pp. 1504–1508, 2014. DOI: <https://doi.org/10.1109/lgrs.2013.2297418>.
- [2] M. Disney, “Terrestrial lidar: A three-dimensional revolution in how we look at trees,” *New Phytologist*, vol. 222, no. 4, pp. 1736–1741, 2019. DOI: <https://doi.org/10.1111/nph.15517>.
- [3] K. Calders *et al.*, “Terrestrial laser scanning in forest ecology: Expanding the horizon,” *Remote Sens. Environ.*, vol. 251, p. 112 102, 2020. DOI: <https://doi.org/10.1016/j.rse.2020.112102>.
- [4] L. Terryn *et al.*, “Tree species classification using structural features derived from terrestrial laser scanning,” *ISPRS J. Photogramm. Remote Sens.*, vol. 168, pp. 170–181, 2020. DOI: <https://doi.org/10.1016/j.isprsjprs.2020.08.009>.

- [5] Z. Xi, C. Hopkinson, S. B. Rood, and D. R. Peddle, “See the forest and the trees: Effective machine and deep learning algorithms for wood filtering and tree species classification from terrestrial laser scanning,” *ISPRS J. Photogramm. Remote Sens.*, vol. 168, pp. 1–16, 2020. DOI: <https://doi.org/10.1016/j.isprsjprs.2020.08.001>.
- [6] D. Seidel *et al.*, “Predicting tree species from 3d laser scanning point clouds using deep learning,” *Frontiers Plant Sci.*, vol. 12, p. 635440, 2021. DOI: <https://doi.org/10.3389/fpls.2021.635440>.
- [7] D. Xu, H. Wang, W. Xu, Z. Luan, and X. Xu, “Lidar applications to estimate forest biomass at individual tree scale: Opportunities, challenges and future perspectives,” *Forests*, vol. 12, no. 5, p. 550, 2021. DOI: <https://doi.org/10.3390/f12050550>.
- [8] B. Brede *et al.*, “Non-destructive estimation of individual tree biomass: Allometric models, terrestrial and uav laser scanning,” *Remote Sens. Environ.*, vol. 280, p. 113180, 2022. DOI: <https://doi.org/10.1016/j.rse.2022.113180>.
- [9] L. Lei *et al.*, “A novel algorithm of individual tree crowns segmentation considering three-dimensional canopy attributes using uav oblique photos,” *Int. J. Appl. Earth Obs. Geoinformation*, vol. 112, p. 102893, 2022. DOI: <https://doi.org/10.1016/j.jag.2022.102893>.
- [10] Y. Cao *et al.*, “Benchmarking airborne laser scanning tree segmentation algorithms in broadleaf forests shows high accuracy only for canopy trees,” *Int. J. Appl. Earth Obs. Geoinformation*, vol. 123, p. 103490, 2023. DOI: <https://doi.org/10.1016/j.jag.2023.103490>.
- [11] J. Trochta, M. Krček, T. Vrška, and K. Král, “3D Forest: An application for descriptions of three-dimensional forest structures using terrestrial LiDAR,” *PLoS one*, vol. 12, no. 5, e0176871, 2017. DOI: <https://doi.org/10.1371/journal.pone.0176871>.
- [12] P. Raunonen, E. Casella, K. Calders, S. Murphy, M. Åkerblom, and M. Kaasalainen, “Massive-scale tree modelling from TLS data,” *ISPRS Ann. Photogramm. Remote Sens. Spat. Inf. Sci.*, vol. 2, no. 3, p. 189, 2015. DOI: <https://doi.org/10.5194/isprsannals-ii-3-w4-189-2015>.
- [13] A. Burt, M. Disney, and K. Calders, “Extracting individual trees from lidar point clouds using treeseg,” *Methods Ecol. Evol.*, vol. 10, no. 3, pp. 438–445, 2019. DOI: <https://doi.org/10.1111/2041-210x.13121>.
- [14] H. Fu, H. Li, Y. Dong, F. Xu, and F. Chen, “Segmenting individual tree from tls point clouds using improved dbscan,” *Forests*, vol. 13, no. 4, p. 566, 2022. DOI: <https://doi.org/10.3390/f13040566>.
- [15] L. Zhong, L. Cheng, H. Xu, Y. Wu, Y. Chen, and M. Li, “Segmentation of individual trees from tls and mls data,” *IEEE J. Sel. Top. Appl. Earth Obs. Remote Sens.*, vol. 10, no. 2, pp. 774–787, 2016. DOI: <https://doi.org/10.1109/jstars.2016.2565519>.
- [16] J. Heinzl and M. O. Huber, “Constrained spectral clustering of individual trees in dense forest using terrestrial laser scanning data,” *Remote Sensing*, vol. 10, no. 7, p. 1056, 2018. DOI: <https://doi.org/10.3390/rs10071056>.
- [17] Z. Xi and C. Hopkinson, “3d graph-based individual-tree isolation (treeiso) from terrestrial laser scanning point clouds,” *Remote Sensing*, vol. 14, no. 23, p. 6116, 2022. DOI: <https://doi.org/10.3390/rs14236116>.
- [18] D. Wang, X. Liang, G. I. Mofack, and O. Martin-Ducup, “Individual tree extraction from terrestrial laser scanning data via graph pathing,” *Forest Ecosystems*, vol. 8, pp. 1–11, 2021. DOI: <https://doi.org/10.1186/s40663-021-00340-w>.
- [19] Q. Liu, W. Ma, J. Zhang, Y. Liu, D. Xu, and J. Wang, “Point-cloud segmentation of individual trees in complex natural forest scenes based on a trunk-growth method,” *J. For. Res.*, vol. 32, no. 6, pp. 2403–2414, 2021. DOI: <https://doi.org/10.1007/s11676-021-01303-1>.
- [20] S. Tao *et al.*, “Segmenting tree crowns from terrestrial and mobile lidar data by exploring ecological theories,” *ISPRS J. Photogramm. Remote Sens.*, vol. 110, pp. 66–76, 2015. DOI: <https://doi.org/10.1016/j.isprsjprs.2015.10.007>.
- [21] D. Wang, “Unsupervised semantic and instance segmentation of forest point clouds,” *ISPRS J. Photogramm. Remote Sens.*, vol. 165, pp. 86–97, 2020. DOI: <https://doi.org/10.1016/j.isprsjprs.2020.04.020>.
- [22] X. Xu, F. Iuricich, K. Calders, J. Armston, and L. De Floriani, “Topology-based individual tree segmentation for automated processing of terrestrial laser scanning point clouds,” *Int. J. Appl. Earth Obs. Geoinformation*, vol. 116, p. 103445, 2023. DOI: <https://doi.org/10.1016/j.jag.2022.103445>.
- [23] O. Martin-Ducup *et al.*, “Evaluation of automated pipelines for tree and plot metric estimation from TLS data in tropical forest areas,” *Ann. bot.*, vol. 128, no. 6, pp. 753–766, 2021. DOI: <https://doi.org/10.1093/aob/mcab051>.
- [24] I. Armeni *et al.*, “3d semantic parsing of large-scale indoor spaces,” in *2016 IEEE Conf. Comput. Vis. Pattern Recognit. (CVPR)*, IEEE, 2016, pp. 1534–1543. DOI: <https://doi.org/10.1109/cvpr.2016.170>.

- [25] A. Dai, A. X. Chang, M. Savva, M. Halber, T. Funkhouser, and M. Nießner, “Scannet: Richly-annotated 3d reconstructions of indoor scenes,” in *2017 IEEE Conf. Comput. Vis. Pattern Recognit. (CVPR)*, IEEE, 2017, pp. 2432–2443. DOI: <https://doi.org/10.1109/cvpr.2017.261>.
- [26] T. Hackel, N. Savinov, L. Ladicky, J. D. Wegner, K. Schindler, and M. Pollefeys, “Semantic3d. net: A new large-scale point cloud classification benchmark,” *arXiv prepr. arXiv:1704.03847*, 2017. DOI: <https://doi.org/10.5194/isprs-annals-iv-1-w1-91-2017>.
- [27] J. Wang *et al.*, “Individual rubber tree segmentation based on ground-based lidar data and faster r-cnn of deep learning,” *Forests*, vol. 10, no. 9, p. 793, 2019. DOI: <https://doi.org/10.3390/f10090793>.
- [28] L. Windrim and M. Bryson, “Forest tree detection and segmentation using high resolution airborne lidar,” in *2019 IEEE/RSJ Int. Conf. Intell. Robots Syst. (IROS)*, IEEE, 2019, pp. 3898–3904. DOI: <https://doi.org/10.1109/iroso40897.2019.8967885>.
- [29] L. Windrim and M. Bryson, “Detection, segmentation, and model fitting of individual tree stems from airborne laser scanning of forests using deep learning,” *Remote Sensing*, vol. 12, no. 9, p. 1469, 2020. DOI: <https://doi.org/10.3390/rs12091469>.
- [30] L. Chang, H. Fan, N. Zhu, and Z. Dong, “A two-stage approach for individual tree segmentation from tls point clouds,” *IEEE J. Sel. Top. Appl. Earth Obs. Remote Sens.*, vol. 15, pp. 8682–8693, 2022. DOI: <https://doi.org/10.1109/jstars.2022.3212445>.
- [31] X. Chen, K. Jiang, Y. Zhu, X. Wang, and T. Yun, “Individual tree crown segmentation directly from uav-borne lidar data using the pointnet of deep learning,” *Forests*, vol. 12, no. 2, p. 131, 2021. DOI: <https://doi.org/10.3390/f12020131>.
- [32] S. Krisanski *et al.*, “Forest structural complexity tool—an open source, fully-automated tool for measuring forest point clouds,” *Remote Sensing*, vol. 13, no. 22, p. 4677, 2021. DOI: <https://doi.org/10.3390/rs13224677>.
- [33] P. Wilkes *et al.*, “Tls2trees: A scalable tree segmentation pipeline for tls data,” *bioRxiv*, pp. 2022–12, 2022. DOI: <https://doi.org/10.1101/2022.12.07.518693>.
- [34] M. Wielgosz, S. Puliti, P. Wilkes, and R. Astrup, “Point2tree (p2t)—framework for parameter tuning of semantic and instance segmentation used with mobile laser scanning data in coniferous forest,” *arXiv prepr. arXiv:2305.02651*, 2023. DOI: <https://doi.org/10.3390/rs15153737>.
- [35] H. Luo, K. Khoshelham, C. Chen, and H. He, “Individual tree extraction from urban mobile laser scanning point clouds using deep pointwise direction embedding,” *ISPRS J. Photogramm. Remote Sens.*, vol. 175, pp. 326–339, 2021. DOI: <https://doi.org/10.1016/j.isprsjprs.2021.03.002>.
- [36] T. Jiang, S. Liu, Q. Zhang, X. Xu, J. Sun, and Y. Wang, “Segmentation of individual trees in urban mls point clouds using a deep learning framework based on cylindrical convolution network,” *Int. J. Appl. Earth Obs. Geoinformation*, vol. 123, p. 103473, 2023. DOI: <https://doi.org/10.1016/j.jag.2023.103473>.
- [37] B. Xiang *et al.*, “Towards accurate instance segmentation in large-scale lidar point clouds,” *arXiv preprint arXiv:2307.02877*, 2023.
- [38] T. Vu, K. Kim, T. M. Luu, T. Nguyen, and C. D. Yoo, “Softgroup for 3d instance segmentation on point clouds,” in *Proc. IEEE/CVF Conf. Comput. Vis. Pattern Recognit.*, 2022, pp. 2708–2717. DOI: <https://doi.org/10.1109/cvpr52688.2022.00273>.
- [39] L. Jiang, H. Zhao, S. Shi, S. Liu, C.-W. Fu, and J. Jia, “Pointgroup: Dual-set point grouping for 3d instance segmentation,” in *Proc. IEEE/CVF conf. comput. vis. Pattern recognit.*, 2020, pp. 4867–4876. DOI: <https://doi.org/10.1109/cvpr42600.2020.00492>.
- [40] J. Sun, C. Qing, J. Tan, and X. Xu, “Superpoint transformer for 3d scene instance segmentation,” *arXiv prepr. arXiv:2211.15766*, 2022. DOI: <https://doi.org/10.1609/aaai.v37i2.25335>.
- [41] J. Schult, F. Engelmann, A. Hermans, O. Litany, S. Tang, and B. Leibe, “Mask3d for 3d semantic instance segmentation,” *arXiv prepr. arXiv:2210.03105*, 2022. DOI: <https://doi.org/10.1109/icra48891.2023.10160590>.
- [42] Y. Wu, M. Shi, S. Du, H. Lu, Z. Cao, and W. Zhong, “3d instances as 1d kernels,” in *Comput. Vision—ECCV 2022: 17th Eur. Conf. Tel Aviv, Isr. Oct. 23–27, 2022, Proceedings, Part XXIX*, Springer, 2022, pp. 235–252. DOI: [https://doi.org/10.1007/978-3-031-19818-2\\_14](https://doi.org/10.1007/978-3-031-19818-2_14).
- [43] T. D. Ngo, B.-S. Hua, and K. Nguyen, “Isbnet: A 3d point cloud instance segmentation network with instance-aware sampling and box-aware dynamic convolution,” *arXiv prepr. arXiv:2303.00246*, 2023. DOI: <https://doi.org/10.1109/cvpr52729.2023.01302>.
- [44] K. Calders, “Terrestrial laser scans—riegl vz400, individual tree point clouds and cylinder models, rushworth forest. version 1. terrestrial ecosystem research network. (dataset).”, 2014. DOI: <https://doi.org/10.4227/05/542B766D5D00D>.



- [45] H. Weiser, J. Schäfer, L. Winiwarter, N. Krašovec, F. E. Fassnacht, and B. Höfle, “Individual tree point clouds and tree measurements from multi-platform laser scanning in german forests,” *Earth Syst. Sci. Data*, vol. 14, no. 7, pp. 2989–3012, 2022. DOI: <https://doi.org/10.5194/essd-14-2989-2022>.
- [46] A. Tockner, C. Gollob, R. Kraßnitzer, T. Ritter, and A. Nothdurft, “Automatic tree crown segmentation using dense forest point clouds from personal laser scanning (pls),” *Int. J. Appl. Earth Obs. Geoinformation*, vol. 114, p. 103 025, 2022. DOI: <https://doi.org/10.1016/j.jag.2022.103025>.
- [47] S. Puliti *et al.*, “For-instance: A uav laser scanning benchmark dataset for semantic and instance segmentation of individual trees,” *arXiv prepr. arXiv:2309.01279*, 2023. DOI: <https://doi.org/10.1109/ccdc52312.2021.9602282>.
- [48] L. C. Neudam *et al.*, “Simulation of silvicultural treatments based on real 3d forest data from mobile laser scanning point clouds,” *Trees, For. People*, p. 100 372, 2023. DOI: <https://doi.org/10.1016/j.tfp.2023.100372>.
- [49] G. Ltd, *Geoslam hub version 6*, Nottingham, UK, 2020. [Online]. Available: <https://geoslam.com>.
- [50] GreenValley International, *Lidar360 point cloud post-processing software*, Accessed: 26.10.2022, 2022. [Online]. Available: <https://greenvalleyintl.com/LiDAR360>.
- [51] Daniel Girardeau-Montaut, *Cloudcompare*, version 2.12.4, Jul. 14, 2022. [Online]. Available: <https://www.cloudcompare.org/>.
- [52] O. Ronneberger, P. Fischer, and T. Brox, “U-net: Convolutional networks for biomedical image segmentation,” in *Int. Conf. Med. Image Comput. Computassist. Interv.*, Springer, 2015, pp. 234–241. DOI: [https://doi.org/10.1007/978-3-319-24574-4\\_28](https://doi.org/10.1007/978-3-319-24574-4_28).
- [53] T. Hackel, J. D. Wegner, and K. Schindler, “Contour detection in unstructured 3d point clouds,” in *Proceedings of the IEEE conference on computer vision and pattern recognition*, 2016, pp. 1610–1618.
- [54] Q.-Y. Zhou, J. Park, and V. Koltun, *Open3D: A modern library for 3D data processing*, 2018. DOI: 10.48550/ARXIV.1801.09847.
- [55] C. R. Qi, O. Litany, K. He, and L. J. Guibas, “Deep hough voting for 3d object detection in point clouds,” in *proc. IEEE/CVF Int. Conf. Comput. Vis.*, 2019, pp. 9277–9286. DOI: <https://doi.org/10.1109/iccv.2019.00937>.
- [56] B. Graham, M. Engelcke, and L. Van Der Maaten, “3d semantic segmentation with submanifold sparse convolutional networks,” in *Proc. IEEE conf. comput. vis. pattern recognit.*, 2018, pp. 9224–9232. DOI: <https://doi.org/10.1109/cvpr.2018.00961>.
- [57] K. He, X. Zhang, S. Ren, and J. Sun, “Deep residual learning for image recognition,” in *Proc. IEEE conf. comput. vis. pattern recognit.*, 2016, pp. 770–778. DOI: <https://doi.org/10.1109/cvpr.2016.90>.
- [58] S. Contributors, *Spconv: Spatially sparse convolution library*, <https://github.com/traveller59/spconv>, 2022.
- [59] M. Ester, H.-P. Kriegel, J. Sander, X. Xu, *et al.*, “A density-based algorithm for discovering clusters in large spatial databases with noise.,” in *kdd*, vol. 96, 1996, pp. 226–231. DOI: <https://doi.org/10.5120/739-1038>.
- [60] I. Loshchilov and F. Hutter, *Decoupled weight decay regularization*, 2017. DOI: 10.48550/ARXIV.1711.05101.
- [61] I. Loshchilov and F. Hutter, *Sgdr: Stochastic gradient descent with warm restarts*, 2016. DOI: 10.48550/ARXIV.1608.03983.
- [62] S. Chen, J. Fang, Q. Zhang, W. Liu, and X. Wang, “Hierarchical aggregation for 3d instance segmentation,” in *Proc. IEEE/CVF Int. Conf. Comput. Vis.*, 2021, pp. 15 467–15 476. DOI: <https://doi.org/10.1109/iccv48922.2021.01518>.
- [63] H. W. Kuhn, “The hungarian method for the assignment problem,” *Nav. res. logist. q.*, vol. 2, no. 1-2, pp. 83–97, 1955. DOI: <https://doi.org/10.1002/nav.20053>.
- [64] K. Calders *et al.*, “Realistic forest stand reconstruction from terrestrial lidar for radiative transfer modelling,” *Remote Sensing*, vol. 10, no. 6, p. 933, 2018. DOI: <https://doi.org/10.3390/rs10060933>.

## A Robustness analysis for grouping radius

The density-based clustering algorithm described in Section 3.4 is controlled by the two hyperparameters  $\tau_{\min}$  and  $\tau_{\text{group}}$ . The selected minimum number of points for a valid cluster  $\tau_{\min} = 100$  is relatively low. Therefore, there is the risk of incurring false positive tree predictions that do not actually constitute a tree but only a fragment of a tree. To counteract the emergence of false positives, the grouping radius can be increased. However, at some point this might lead to false negative predictions due to tree clusters merging together. To quantify this trade-off between false positives and false negatives, we conducted an experiment where we vary the grouping radius  $\tau_{\text{group}}$  between 2.5 cm and 70 cm and measure the corresponding detection failures. For the fine-tuned model, the expected tendency for clusters to break apart could be observed for a very small grouping radius of 2.5 cm, while this was not the case for the model trained on noisy labels (Figure 8, green line). This can be attributed to the fact that, in the fine-tuned setting, a single tree-cluster is more likely to be split into distinguishable sub-clusters due to a more precise offset prediction. Furthermore, the expected tendency for clusters to merge could be observed for both settings (Figure 8, red line). However, the number of detection failures is in general very low and not strongly influenced by changes in the grouping radius, which suggests that our method is robust to changes in this hyperparameter. For practical purposes, we recommend setting the grouping radius relatively low (somewhere in the range of 0.1 m to 0.2 m) since false positives can be easily dealt with by simply merging fragments together, while merged trees cannot be that easily recovered.

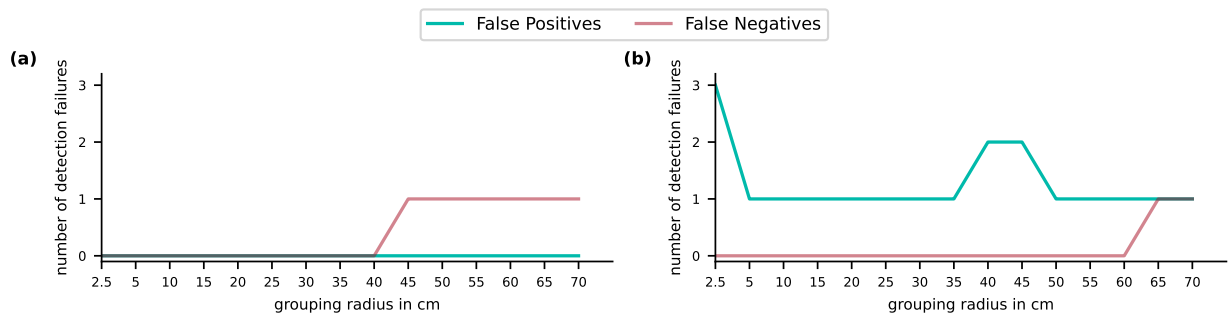


Figure 8: Number of false positive and false negative tree predictions depending on the grouping radius for (a) the non-fine-tuned model and (b) the fine-tuned model.